# Stokes trap for multiplexed particle manipulation and assembly using fluidics

Anish Shenoy[a], Christopher V. Rao[b], and Charles M. Schroeder[b,c,1]

[a]Department of Mechanical Science and Engineering, University of Illinois at Urbana–Champaign, Urbana, IL 61801; [b]Department of Chemical and Biomolecular Engineering, University of Illinois at Urbana–Champaign, Urbana, IL 61801; and [c]Center for Biophysics and Computational Biology, University of Illinois at Urbana–Champaign, Urbana, IL 61801

Edited by David A. Weitz, Harvard University, Cambridge, MA, and approved March 1, 2016 (received for review December 20, 2015)

**The ability to confine and manipulate single particles and molecules has revolutionized several fields of science. Hydrodynamic trapping offers an attractive method for particle manipulation in free solution without the need for optical, electric, acoustic, or magnetic fields. Here, we develop and demonstrate the Stokes trap, which is a new method for trapping multiple particles using only fluid flow. We demonstrate simultaneous manipulation of two particles in a simple microfluidic device using model predictive control. We further show that this approach can be used for fluidic-directed assembly of multiple particles in solution. Overall, this technique opens new vistas for fundamental studies of particle–particle interactions and provides a new method for the directed assembly of colloidal particles.**

microfluidics | trapping | directed assembly | Stokes | hydrodynamic

In recent years, particle-trapping methods have enabled a multitude of fundamental studies in the natural and applied sciences. To this end, the precise manipulation of small particles and single molecules has opened new windows into viewing biological and physical processes with unprecedented levels of control. Nearly all trapping methods rely on a fundamental set of forces for particle confinement, with techniques including optical traps (1–3), magnetic traps (4), acoustic traps (5, 6), electrokinetic traps (7, 8) and the hydrodynamic trap (9–11). Using these methods, researchers have studied phenomena ranging from the cooling of atoms to low temperatures (12) to the mechanistic behavior of single biomolecules (13).

Particle-trapping methods can be characterized by the nature of the underlying forces and the action of confinement. Trapping techniques can be broadly classified as passive (non–control-based) or active (control-based) traps. Passive traps allow for particle confinement over long periods of time without the need for active feedback control (e.g., optical traps), wherein a stable potential well is used to generate a restoring force to confine a particle at or near a target location. Active traps use a feedback-control algorithm for particle trapping, wherein disturbances such as thermal fluctuations can be corrected using active feedback control (e.g., electrokinetic or hydrodynamic traps). Despite the pervasive use of particle trapping techniques for fundamental investigations, several methods require complex experimental setups and impose specific restrictions on the properties of the trapped particle and the surrounding medium (e.g., dielectric constants or ionic strength). On the other hand, hydrodynamic traps impose no specific constraints on a particle's surface chemistry, morphology, or refractive index (14). From this perspective, hydrodynamic methods possess several advantages for particle trapping and manipulation, and yet this approach has not yet been extended to multiple particles.

In 1934, G. I. Taylor developed the first active trap based on hydrodynamic flow (15). The four-roll mill was able to confine single macroscopic particles or immiscible droplets by continuous rotation of four cylinders, thereby generating a stagnation point flow. The original four-roll mill relied on manual (human) feedback control for particle confinement, which limits precision and controllability. In 1986, Bentley and Leal developed an automated four-roll mill by controlling the rotational speeds of the rollers using a computer (16). The automated four-roll mill, however, was based on a "macrofluidic" experimental flow cell, which complicates the confinement of small particles because of finite system response times. In recent years, the advent of microfluidics has allowed for fabrication of flow devices with small feature sizes, thereby enabling dynamic fluidic control with correspondingly small timescales. In 2003, a microfluidic cross-slot device was used to trap single DNA molecules near the stagnation point of a planar extensional flow, albeit using manual (tedious) human control over hydrostatic pressure in the outlet flow channels (17). A microfluidic four-roll mill was also developed and shown to generate extensional, rotational, and linear mixed flows (18, 19); however, these devices lack feedback control, which precludes long-term confinement of single particles and molecules.

In 2010, Schroeder and coworkers built and demonstrated an automated hydrodynamic trap capable of confining single particles at a target position for several minutes in a polydimethylsiloxane (PDMS)-based microfluidic device (9). In this device, an on-chip membrane valve was used to modulate flow rate in one outlet channel, thereby enabling particle trapping near a stagnation point for long times (10). By incorporating multiple on-chip valves, it was shown that single particles can be precisely manipulated in two dimensions using the sole action of fluid flow (11). In all cases, the automated hydrodynamic trap relies on a simple proportional-integral-derivative (PID) controller for particle manipulation (10, 20), which was sufficient for precise confinement of small particles in solution (e.g., 500-nm particles confined to within 180 nm of a set point position) (11). Despite these advances, however, the original automated hydrodynamic trap is strictly limited to trapping and manipulation of single particles. From this perspective, there is a strong need for new fluidic-based methods for precise confinement of multiple particles in solution. The ability to manipulate multiple particles in solution using simple microfluidics will enable a wide array of fundamental studies of particle–particle interactions and particle assembly. In particular, flow-based control over multiple particles will allow for detailed studies of soft particle interactions,

## Significance

**In recent years, techniques for trapping and manipulating small particles and single molecules have catalyzed major advances in several fields of science. Here, we describe a new method for confining, manipulating, and assembling multiple particles in free solution using the sole action of fluid flow. The Stokes trap provides a fundamentally new method for particle manipulation and assembly using a simple microfluidic device and nonlinear feedback control in the absence of optical, electric, or magnetic fields. This method holds strong potential to enable fundamental studies in soft materials, colloidal science, and biophysics.**

Author contributions: A.S. and C.M.S. designed research; A.S. performed research; C.V.R. contributed new reagents/analytic tools; A.S. analyzed data; and A.S., C.V.R., and C.M.S. wrote the paper.

The authors declare no conflict of interest.

This article is a PNAS Direct Submission.

[1]To whom correspondence should be addressed. Email: cms@illinois.edu.

This article contains supporting information online at www.pnas.org/lookup/suppl/doi:10.1073/pnas.1525162113/-/DCSupplemental.

including vesicle fusion, drop coalescence, and multiphase fluid interactions in small drops or particles.

In this work, we describe the Stokes trap, which is a new method for the manipulation of multiple particles using the sole action of fluid flow. The Stokes trap relies on precise control over particle position in viscous-dominated (low-Reynolds number) flows. Although prior work considered an open-loop algorithm for microfluidic assembly (21), this method was solely focused on computational studies of non-Brownian particles. Here, we develop and experimentally demonstrate a highly robust and scalable closed-loop control strategy that enables the precise manipulation of multiple particles and fluidic directed assembly of multiple particles.

## Modeling and Design of the Stokes Trap

**Fluidic Model and Governing Equations.** Consider the problem of manipulating $P$ particles independently in a microfluidic device in which $N$ channels intersect to form an $N$-sided polygonal flow device (Fig. 1*A* shows cross-slots with $N=4$ and $N=6$) (21). The objective is to control the 2D center-of-mass position of each particle, which requires controlling $2P$ variables simultaneously. The control (or input) to this microfluidic system is the time-dependent flow rates within the $N$ channels. Because of conservation of mass, however, we can only prescribe $N-1$ flow rates independently because the net mass flow rate into the microdevice must be zero. To properly control multiple particles, we need at least as many control variables in the system as there are degrees of freedom, hence $N \geq 2P+1$. Therefore, a four-channel microfluidic device can trap a single particle, which is consistent with prior work (11). Nevertheless, the simple cross-slot design used in the (Generation I) automated hydrodynamic trap does not have the required degrees of freedom for $P \geq 2$ particles.

We first consider the fluid dynamics within the microfluidic device. At low Reynolds number (Stokes flow conditions), we can neglect fluid inertia which yields the following conservation equations (22):

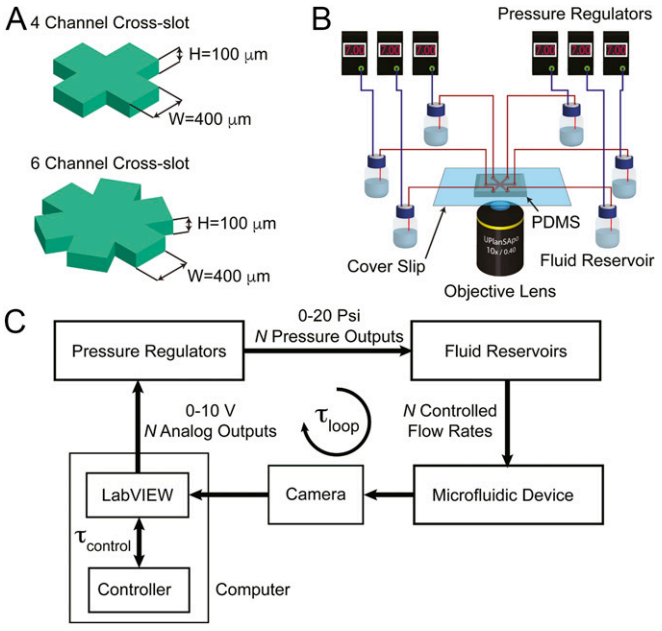


**Fig. 1.** Overview of the Stokes trap and control algorithm. (*A*) Schematics of four-channel and six-channel microfluidic devices for manipulating one and two particles, respectively. (*B*) Overview of the experimental setup. Inlet/outlet channels in the microfluidic device are connected to fluidic reservoirs that are pressurized by regulators controlled by a custom LabVIEW program. In this way, the fluidic reservoirs drive fluid flow in the microdevice. (*C*) Block diagram of the control loop for particle manipulation and trapping, with typical time constants of $\tau_{loop}$ = 33 ms and $\tau_{control}$ = 500 μs.

$$\nabla \cdot \mathbf{v} = 0, \qquad -\nabla p + \mu \nabla^2 \mathbf{v} + \rho \mathbf{b} = 0, \qquad [1]$$

where $\mathbf{v}$ is fluid velocity, $p$ is pressure, μ is viscosity, $\rho$ is density and $\rho\mathbf{b}$ is a volumetric (body) force. In typical microfluidic devices, the vertical channel height $H$ is much smaller than channel width $W$ such that $H < W$. The velocity profile is parabolic in the vertical direction, with the height-averaged velocity being proportional to the gradient of pressure. Using the formalism of a Hele-Shaw flow cell (22), each inlet channel is approximated as a point source, and the height-averaged fluid velocity inside the cross-slot is expressed as a linear superposition of $N$ source flows (21):

$$\mathbf{v}(\mathbf{x}) = \frac{1}{\pi H} \sum_{i=1}^{N} \frac{(\mathbf{x}-\mathbf{R}_i)}{\|\mathbf{x}-\mathbf{R}_i\|^2} q_i, \qquad [2]$$

where $\mathbf{R}_i \in \mathbb{R}^2$ is the position vector of the point source corresponding to the $i^{th}$ channel, and $\mathbf{q} \in \mathbb{R}^N$ is a vector containing flow rates whose $i^{th}$ element is the flow rate through the $i^{th}$ channel. This equation represents the Hele-Shaw velocity field because of point sources in an unbounded 2D domain and is an approximation to the actual flow field. In reality, the microfluidic cross-slot is a bounded 3D domain. The point source is also semicircular in nature as the fluid can only flow into a semicircular region inside the cross-slot, which leads to the prefactor of $1/\pi H$ by applying mass conservation. Of course, the choice of $q_i$ must satisfy mass conservation such that

$$\sum_{i=1}^{N} q_i = 0, \qquad [3]$$

where flow into the cross-slot is defined to be positive $(q > 0)$. We validated the point source model by determining the velocity field inside a 3D microfluidic polygonal geometry using computational fluid dynamics (COMSOL). The height-averaged fluid velocity was compared with our model (Eq. **2**) as a function of position inside the microdevice (*SI Appendix*, *SI Text*, *1.1. Device Design and Fabrication* and *1.2. COMSOL Simulations*). In general, we found that this model accurately captures the fluid flow profiles in the device (to within ∼2%), and minor deviations can be reduced by choosing an aspect ratio of ∼1:4 for the channels.

Using this model, the fluid velocity at a point inside the polygonal device is completely determined by the imposed flow rates $q_i$. Let us assume that a particle is advected with the same local velocity as the fluid, such that the particle's center-of-mass velocity is given by Eq. **2**. It is then possible to invert Eqs. **2** and **3** to obtain the flow rates $q_i$ required to achieve a set of desired particle velocities. Let the instantaneous position of the particle be $\mathbf{x} \triangleq [x,y]^T \in \mathbb{R}^2$. The governing equations for the particle are

$$\frac{d\mathbf{x}}{dt} = \mathbf{F}(\mathbf{x},\mathbf{q},\mathbf{R}) \triangleq \frac{1}{\pi H} \sum_{i=1}^{N} \frac{(\mathbf{x}-\mathbf{R}_i)}{\|\mathbf{x}-\mathbf{R}_i\|^2} q_i, \qquad [4a]$$

$$\sum_{i=1}^{N} q_i = 0. \qquad [4b]$$

Although it is possible to completely determine the set of flow rates $q_i$ via matrix inversion, this method is generally not practical for experiments because of unreasonably large fluxes required for certain scenarios such as close approach of two particles. To circumvent this issue, we use a control algorithm for determining $q_i$.

**Model Predictive Control.** Given the governing equations for fluid flow, the next challenge lies in implementing a control algorithm to determine experimentally feasible flow rates $q_i$ to manipulate

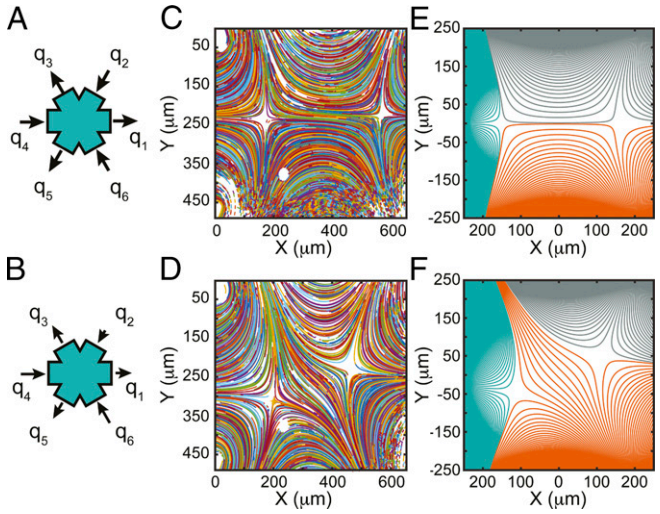


**Fig. 2.** Streamline topologies in a six-channel microdevice from experiments and computation. (*A* and *B*) Schematic of the relative magnitude and direction of the flow rates for generating the streamline topologies in the figures below. Arrows pointing inwards represent flow entering the device, and arrows pointing outwards represent flow exiting the device. The size of the arrows signifies the relative magnitude of the flow rates. (*C*) Experimental streamlines showing the linked-arms topology, generated when the flow rates have a specific symmetry. Two stagnation points are clearly visible. (*D*) Experimental streamlines showing the non–linked-arms topology, generated if the symmetry in *C* is broken. (*E* and *F*) Streamline topologies obtained from numerical solution of Eq. **2**. For display, streamlines emanating from inlet channels are plotted using distinct colors.

particles. In a recent computational study on particle assembly (21), the flow rates required for maneuvering particles were obtained by minimizing an objective function using Pontryagin's maximum principle. However, this approach assumes that particles are non-Brownian and therefore move deterministically with the flow; moreover, this approach does not consider perturbations in flow rates or modeling inaccuracies that may arise naturally in experiments.

Steering a single particle from an initial position $\mathbf{x}^0$ to the final position $\mathbf{x}^F$ requires imposed flow rates that vary with time and involves several experimental challenges. First, we aim to confine and manipulate Brownian particles (<10 μm in diameter) for which thermal fluctuations are significant, thereby yielding stochastic, nondeterministic particle trajectories. Second, it is possible that the fluidic model described by Eq. **2** may differ from the actual experimental flow field because of modeling inaccuracies and/or actuator resolution limits, which necessitates the use of a robust control algorithm. Third, we found that solution of adjoint equations was computationally intensive and not well suited for real-time experimental implementation. In our work, we aim to solve the system equations on the millisecond timescale at typical acquisition rates of 30 Hz, which necessitates a robust control strategy that can rapidly solve the governing equations. For these reasons, we implement a model predictive control (MPC) algorithm for precise control (23).

We briefly discuss the MPC strategy followed by experimental implementation. First, a finite time horizon $[0, T]$ is selected and divided into a discrete number of intervals $M$ of equal size, such that each interval is equal to the sampling time. The imposed flow rates are assumed to be piecewise constant during each interval but change from one interval to the next. Next, a matrix of flow rate vectors is defined for each interval in the time horizon such that $\mathbf{Q} = [\mathbf{q}^1, \mathbf{q}^2, \ldots, \mathbf{q}^M]$. Given a certain combination of flow rates over the horizon and the current position $\mathbf{x}^0$, we can calculate the trajectory of the particle over the time horizon by numerically solving Eq. **2**. We discretize the trajectory at the endpoints of each interval, denoting the position of the particle at these points as $\mathbf{X} = [\mathbf{x}^0, \mathbf{x}^1, \ldots, \mathbf{x}^M]$. We also define an integrator variable $\mathbf{e}$, such that $d\mathbf{e}/dt = \mathbf{x} - \mathbf{x}^F$, with a corresponding matrix $\mathbf{E} = [\mathbf{e}^0, \mathbf{e}^1, \ldots, \mathbf{e}^{M-1}]$.

For the general case of trapping $P$ particles, we redefine the state vector $\mathbf{x} \triangleq [\mathbf{x}_1^T, \mathbf{x}_2^T, \ldots, \mathbf{x}_P^T]^T$, so that the vector contains the position vector of each particle. We seek to determine particle trajectories that minimize distance traveled while also minimizing flow rates, where the latter condition ensures that the flow rates have physically realizable values in experiments and that the optimization problem is well posed. However, not all trajectories from the initial position $\mathbf{x}^0$ to the final positions $\mathbf{x}^F$ are feasible or desirable, because some trajectories might violate mass conservation or take a circuitous path. To systematically obtain optimal trajectories and flow rates, $\mathbf{Q}$ is expressed as the argument of an optimization problem:

$$\min_{\mathbf{X},\mathbf{E},\mathbf{Q}} J = \sum_{k=0}^{M-1} \left\{ \alpha\left( \left\| \mathbf{x}^k - \mathbf{x}^F \right\|^2 \right) + \beta \left\| \mathbf{q}^k \right\|^2 + \delta \left\| \mathbf{e}^k \right\|^2 \right\} + \gamma\left( \left\| \mathbf{x}^M - \mathbf{x}^F \right\|^2 \right), \quad [5a]$$

$$\text{s.t.} \quad \frac{d\mathbf{x}}{dt} = \left[ \mathbf{F}^T(\mathbf{x}_1, \mathbf{q}, \mathbf{R}), \ldots, \mathbf{F}^T(\mathbf{x}_P, \mathbf{q}, \mathbf{R}) \right]^T, \quad \mathbf{x}(0) = \mathbf{x}^0, \quad [5b]$$

$$\frac{d\mathbf{e}}{dt} = \mathbf{x} - \mathbf{x}^F, \quad [5c]$$

$$\sum_{i=1}^{N} q_i = 0, \quad [5d]$$

where $J$ is the objective function and $\alpha$, $\beta$, $\gamma$, and $\delta$ are scalar weights that can be dynamically tuned to obtain the desired response, for example, removing the offset between the desired target position and the current position.

By solving the optimization problem, we obtain flow rates $\mathbf{Q}$ that move a particle from its current position to a target position at a minimal cost, as determined by the weighting factors. However, in our approach, we only apply the first set of flow rates $\mathbf{q}^1$ from the calculated $\mathbf{Q}$, and then we remeasure the $\mathbf{x}^0$ after one sampling period (i.e., $T/M$ seconds) which becomes the initial condition for the optimization problem at the next sampling instant. In this way, flow rates are calculated for the entire trajectory over the horizon, but only the flow rates for the first interval are applied, at which point the particle position is remeasured. This process is repeated continuously throughout the experimental period. The MPC strategy is highly tolerant to fluctuations and experimental perturbations described above. Here, we implement MPC using the Automatic Control and Dynamic Optimization

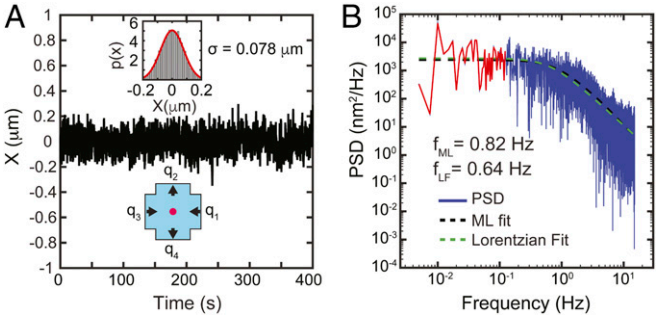


**Fig. 3.** Characterizing the performance of the Stokes trap. (*A*) Trajectory of trapped 2.2-μm-diameter bead over a period of 400 s. (*Inset, Upper*) Probability distribution of the position of the particle. (*Inset, Lower*) Schematic of microdevice used for trapping. (*B*) PSD particle position fluctuations for the trajectory shown in *A*. The PSD is analyzed to determine the corner frequency $f_c$.

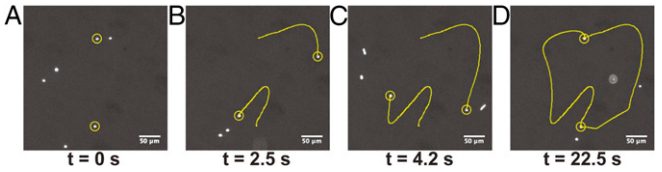


**Fig. 4.** Manipulating two particles using the Stokes trap, where the objective is to switch the center-of-mass positions of both particles. (*A*) At $t = 0$ s, two 2.2-μm-diameter fluorescent beads are initially trapped ∼198 μm apart. At $t = 0.033$ s, we instantaneously interchange the target positions of both particles, after which the controller generates a trajectory for each particle and calculates and applies the flow rates. (*B* and *C*) Tracing the two particle trajectories during the experiment, with the yellow line showing the past history of both particles. (*D*) The process finishes at $t = 22.5$ s, at which time the particle positions have been interchanged.

(ACADO) toolkit (*SI Appendix, SI Text, 1.3. Controller Implementation*) (24).

## Results

**Stokes Trap: Overview and Design.** A schematic illustration of the four- and six-channel microdevices is shown in Fig. 1*A*. In these experiments, we use a four-channel device for trapping a single particle and a six-channel device for trapping two particles. For trapping two particles, we found that an additional control variable $(N = 6)$ provides more flexible control, even though the system has $2P + 1 = 5$ degrees of freedom in this case. Fig. 1*B* shows a schematic of the overall experimental setup for the Stokes trap. The setup consists of 6 pressure regulators that control fluid flow by pressurizing six distinct fluid reservoirs, which are in turn connected to a microfluidic device mounted on the stage of an inverted microscope. The Stokes trap operates at a net-positive pressure such that each fluidic channel can function as an inlet or outlet channel with net-positive or net-negative flux, respectively, by simply varying pressure (*SI Appendix, SI Text, 1.3. Controller Implementation*). A schematic block diagram showing implementation of the control loop is shown in Fig. 1*C*. The algorithm begins when a CCD camera acquires a snapshot and relays the image to a custom LabVIEW program. Next, LabVIEW localizes particles and determines the 2D center-of-mass coordinates of target particle(s). The LabVIEW program allows the user to dynamically set the target set point positions for both particles through a graphical user interface (GUI). Next, the particles' coordinates are transmitted to the ACADO controller to determine the requisite flow rates for steering the particles to the desired positions. In this step, the controller solves Eq. **5** to obtain the set of flow rates $q_i$ for each channel and transmits the information back to LabVIEW. Finally, LabVIEW converts these flow rates to corresponding pressures and actuates the pressure regulators, which deliver the required flow rates to the device via the fluid reservoirs.

**Fluidic Model and Streamline Topologies.** Before embarking on particle trapping, we first validated the fluidic model (Eq. **2**) by experimentally determining streamline topologies using particle tracking and fluorescence microscopy. In these experiments, we use an aqueous glycerol buffer (viscosity, $\eta = 12.6$ cP) containing 2.2-μm-diameter fluorescent beads to characterize the flow field. We use standard bead tracking algorithms [ImageJ with MOSAIC plugin (25)] to determine bead trajectories over at least 30-s durations, which is suitable for quantitative flow field analysis at typical strain rates of 1–10 $s^{-1}$. Fig. 2 *A* and *B* illustrates the direction and magnitude of the imposed flow rates in the six-channel device during these experiments. Experimental streamline topologies are plotted in Fig. 2 *C* and *D*. Interestingly, we observe two distinct flow topologies to which we refer as "linked-arms" (Fig. 2*C*) and "non–linked-arms" topologies (Fig. 2*D*). In both cases, we clearly observe the existence of two stagnation points, which facilitates the independent trapping of two particles. In the linked-arms topology, we observe that the principal axis of extension for the right stagnation point corresponds to the principal axis of compression for the left stagnation point. In the non–linked-arms topology, the stagnation points are no longer connected by streamlines. We obtained similar streamline topologies by numerically solving Eq. **2**, as shown in Fig. 2 *E* and *F*.

**Trapping Single Particles Using the Stokes Trap.** We first characterized the performance of the Stokes trap by confining single particles at a target position and determining the trap stiffness. The Stokes trap can be used to confine particles in either quiescent conditions (i.e., no net flow if the particle is at the target position) or in net-flow conditions (i.e., net flow even if the particle is at target position). In quiescent conditions, fluid flow is only applied to correct for the Brownian motion of the particle, and in this case, the Stokes trap functions in an analogous fashion to electrokinetic traps (7). As an aside, we note that unlike the Stokes trap, the Generation I automated hydrodynamic trap cannot operate under quiescent conditions. The Generation I trap uses an on-chip membrane valve to control flow, and the membrane valve is incapable of influencing particle position in the absence of a net imposed flow.

To quantify trap performance, we used the Stokes trap with MPC (Eq. **5**) to confine a single (2.2-μm-diameter) fluorescent bead in a four-channel device, and we recorded the particle trajectory for a duration of 400 s (Fig. 3*A*). We use a bead-tracking algorithm to localize particle position, followed by determination of the power spectral density (PSD) of the particle position fluctuations (Fig. 3*B*). We fit the PSD with a Lorentzian and a maximum-likelihood estimator (26, 27), and the corner frequency $f_c$ was determined to be 0.64 and 0.82 Hz using these methods, respectively. We determined the trap stiffness $\kappa = 2\pi\zeta f_c$ as $1.1 \times 10^{-3}$ pN/nm and $1.3 \times 10^{-3}$ pN/nm, where $\zeta$ is the Stokes drag of the bead. These trapping stiffnesses are comparable to a weak optical trap (28). Moreover, we found that the MPC algorithm and the overall design of the Stokes trap yields a tighter trap (∼5–7× increase in trap stiffness) compared with the previous Generation I automated hydrodynamic trap, which only used a simple proportional controller and an on-chip valve to yield a stiffness of $2.0 \times 10^{-4}$ pN/nm under similar experimental conditions (9).

**Manipulating Two Particles Using the Stokes Trap.** We next used the Stokes trap to confine and manipulate two particles simultaneously (Fig. 4). Here, we used a six-channel microfluidic device to

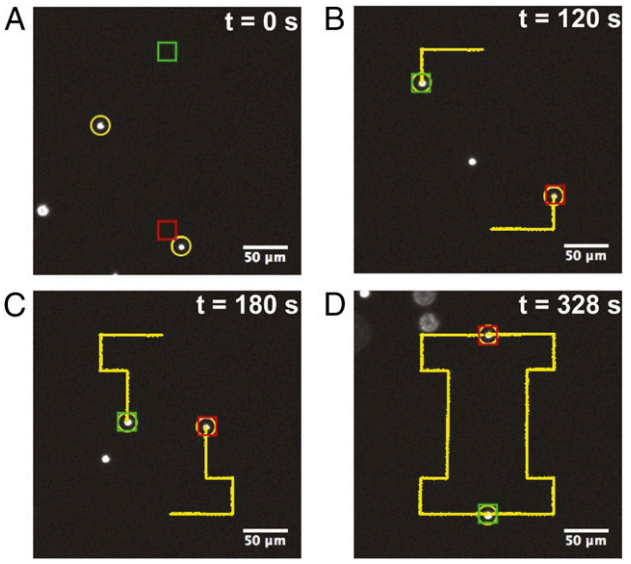


**Fig. 5.** Manipulating two particles using the Stokes trap, where the objective is to precisely control the paths of two 2.2-μm beads to trace the letter I. (*A–D*) Snapshots of both particles at various instants of time, with the yellow line showing the past history of both particles.

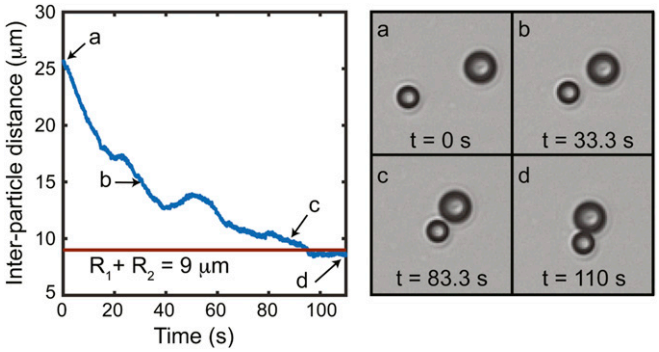


**Fig. 6.** Fluidic-directed assembly of two particles using the Stokes trap. Interparticle distance is shown as a function of time during the assembly event between a 10.6-μm-diameter streptavidin-coated bead and a 7.4-μm-diameter biotin-coated bead. (*Right*) Snapshots of both particles as a function of time, where points a to d correspond to the interparticle distance plot. The beads are successfully linked around 95 s.

manipulate two 2.2-μm-diameter particles in an arbitrary scenario. First, the two particles are trapped ∼198 μm apart. Next, the target positions of both particles are instantaneously interchanged, and the MPC given by Eq. **5** is used to control the process of particle interchange. In this experiment, we do not prescribe the intermediate trajectory for either particle; rather, the trajectory is generated by the controller. We found that the controller successfully generates smooth trajectories in real time by minimizing the objective function, as shown in Fig. 4. Using this strategy, the particle-position interchange occurs over a relatively short timescale, with the entire process completing in 22.5 s (Movie S1).

We further demonstrate the precise manipulation of two particles along preprogrammed paths (Fig. 5 and *SI Appendix*, Fig. S4). The experiment begins by tracking two freely suspended particles in the field of view, and at time $t = 0$ s, the controller is activated. First, the controller traps both particles, and the two particles are smoothly delivered to their respective (initial) target positions. Next, the target position is slowly and repeatedly stepped along a preprogrammed path, during which time the controller works to continuously move the particles synchronously with the target position. In this experiment, the target positions are programmed to trace the letter I, and the process completes after 328 s. As shown in Fig. 5, we are able to accurately and precisely control both particles along a predetermined path that spans hundreds of microns, which is orders of magnitude larger than the particle size (Movie S2).

**Fluidic-Directed Assembly of Particles.** We also used the Stokes trap to assemble two small particles in solution (Fig. 6). In this experiment, the goal is to link two "sticky" particles together via directed assembly, in particular by linking a 7.4-μm biotin-coated bead and a 10.6-μm streptavidin-coated bead by the strong noncovalent biotin–streptavidin interaction. At time $t = 0$ s, both particles are trapped at two separate positions. Next, the target position for the bead on the left (biotin-coated) is slowly moved toward the target position for the bead on the right (streptavidin-coated). As the beads approach each other, both particles begin to deviate from their target positions, which is a consequence of interparticle hydrodynamic interactions (22, 29). Nevertheless, particles follow their target positions at all interparticle distances using the MPC algorithm. For assembly experiments, the controller weight parameter γ in the objective function (Eq. **5**) is increased slightly above the values used in two particle manipulation experiments described above, which amounts to a stricter penalization for not reaching the final target position. At $t =$ 95 s, the two beads are firmly linked together by biotin–streptavidin interaction. The interparticle distance during the assembly event is plotted in Fig. 6, with snapshots of both particles shown on the right. For reference, the expected interparticle distance after linking is also plotted on the same figure. After linking the two particles together, we moved the assembled structure around in solution to confirm that the beads were tightly linked (Movie S3).

## Discussion

In this paper, we demonstrate a new technique for manipulating and assembling microscale objects in free solution using the sole action of fluid flow. We experimentally implement model predictive flow control, which greatly simplifies the microfluidic device design for trapping by eliminating the need for integrated electrodes and on-chip membrane valves. The MPC algorithm is versatile and allows for the ability to control several particles independently, and as a proof of concept, we directly show the precise manipulation of two particles along arbitrary paths. We further use this technique to bring two particles in close contact, thereby facilitating linkage and directed assembly into a simple structure. Although simultaneous manipulation of multiple particles has been achieved using optical tweezers (2) and electrokinetic traps (8), multiparticle manipulation and assembly mediated only by fluid flow has not yet been achieved.

A major advantage of the MPC algorithm is the ability to correct for model imperfections and system perturbations in a robust manner. For example, our simple fluidic model for fluid velocity (and particle velocity) is based on a linear superposition of 2D point source flows around the perimeter of a polygonal flow cell. This model neglects interparticle hydrodynamic interactions, which give rise to perturbations in the fluid velocity that become significant upon close approach of the particles (e.g., when interparticle distance is less than ∼5 particle diameters). Nevertheless, as shown in the particle assembly experiment, the MPC algorithm is robust and successfully corrects limitations of the fluidic model.

A second advantage of implementing the MPC algorithm with distinct fluidic models is the ability to directly measure deviations of the system behavior from the model predictions. During an experiment, we record the transient and steady-state control input that effectively cancels any perturbations to the flow field. Interestingly, this approach allows for direct measurement of the fluid velocity arising from the flow field disturbances around trapped particles. In this manner, it should be possible to use one particle as a probe particle to record the fluid flow in the vicinity of a second particle. Thus, we believe that this technique can serve as a powerful tool to study interparticle interactions.

We anticipate that the Stokes trap can be used to study fundamental interactions between hard or soft particles, including vesicle fusion, polymersome fusion, droplet coalescence, coacervate droplet interactions and disassembly, red blood cell collisions, and interactions between living cells. Indeed, the Stokes trap places no restrictions on the physical properties of trapped particles (e.g., no restrictions on index of refraction or magnetic susceptibility), aside from the need to image particles. This versatility greatly extends the range of applicability of the method to a wide variety of studies, including manipulation of hard colloids, anisotropic particles, or soft particles. For example, our technique could serve as an alternative to micropipette aspiration in the study of cell adhesion, wherein one cell is typically confined using a small pipette before probing cell–cell interactions, a process that may perturb cell properties via physical confinement. Furthermore, fluidic trapping generally involves application of gentle, viscous-dominated flows that result in nonperturbative forces, thereby enabling trapping of particles ranging from nanometer-sized inorganic particles to giant vesicles, all with using a simple and robust modular setup. Moreover, fluidic confinement forces scale favorably and linearly with particle diameter $R$ compared with $R^3$ for optical traps and magnetic tweezers, which implies that the forces required for trapping a small particles using fluidics are physically reasonable given typical experimental conditions (8). In addition, coupling external optical and electrical fields into microfluidic devices often has associated side effects such as secondary flows generation and localized heating (30), which could complicate the study of biological molecules and cells using these methods.

We further use the Stokes trap for the assembly of freely suspended particles in solution, that is, for particles with no

external force or torque couples (e.g., no external electric fields or optical fields). In recent years, self-assembly of particles and molecules has been used to generate advanced functional materials with hierarchical structures (31). The process of self-assembly, however, mainly relies on self-organization at thermal equilibrium (32). From this perspective, it might be possible to access new levels of spatial ordering and hierarchical assembly by coupling external fields during the assembly process in a nonperturbative fashion. In the past, directed assembly of colloidal particles has been achieved by using external electrical fields (33, 34), acoustic fields (35), or optical fields (36). Nevertheless, not all techniques are well suited for directed assembly. Particle assembly with electrokinetic traps has been shown to be difficult, where the electrode potentials (voltages) required for bringing two 5-μm particles in contact diverged upon close approach, and as a consequence, these particles could not be brought closer than ∼8 μm (8). Moreover, during any assembly event, the applied force fields should be nonperturbative such that they do not alter the underlying system properties.

Despite its advantages, the Stokes trap has a few disadvantages for particle trapping. In the current implementation, we only control motion in the *x*-*y* plane, with no control over the position in the *z* direction. In addition, trapping occurs at an unstable equilibrium position in flow, which necessitates trapping via active feedback control, rather than passive trapping as achieved in optical traps.

In future work, it may be possible to use the Stokes trap to systematically build higher-order and more complex assemblies of particles. In the current version of the trap, we use $n = 6$ inlet/outlet channels, though it has been predicted that this can be scaled up to $n$ = 10–15 while retaining controllability with physically reasonable flow rates (21). In the short term, however, the current device with $n = 6$ control variables could be used to control the 2D center-of-mass position of two particles while simultaneously controlling the orientation of one of the two particles. By adding one additional channel ($n = 7$), it would be straightforward to control the 2D orientation and center-of-mass position of two anisotropic particles.

## Materials and Methods

**Microfluidic Device Fabrication.** Standard procedures for PDMS-based soft lithography were followed to fabricate four- and six-channel microdevices (*SI Appendix, SI Text, 1.1. Device Design and Fabrication*).

**Experimental Setup and Sample Preparation.** The microfluidic device was mounted on the stage of an inverted microscope (Olympus IX71) equipped with a 10× objective lens and a CCD camera (AVT Stingray F-033B/Point Gray GS3). The inlet/outlet channels on the microdevice were connected to fluidic reservoirs (Elveflow) through FEP tubing (IDEX Health & Science), and the reservoirs were pressurized using electronic pressure regulators (Proportion Air). In all experiments, the buffer is a glycerol–water solution with a viscosity of 12.6 Pa-s at room temperature (25 °C). For trapping experiments, we used 2.2-μm-diameter fluorescent polystyrene beads (Nile Red; Spherotech). For assembly experiments, we used 10.6-μm and 7.4-μm-diameter polystyrene beads coated with streptavidin and biotin (Spherotech and Bangs Laboratories, respectively).

**Scaling and Nondimensionalization.** The optimization problem (Eq. **5**) is solved numerically in real-time during experiments, and it is important to scale all quantities to be $O(1)$. We define a characteristic timescale $t_c$ as the time required to replace the volume of fluid inside the flow chamber at a characteristic flow rate $q_c$ such that $t_c = \pi R^2 H/q_c$, where $H$ is the channel height and $R = W$ is the radius of the circle circumscribing the hexagonal fluid chamber, where $W$ is the inlet channel width. We define a characteristic flow rate $q_c$ = 0.5 μL/h and a characteristic length scale $l_c = R$. These definitions yield a characteristic velocity of $v_c = R/t_c$. All controller equations are scaled using these variables, such that Eq. **4** becomes $\bar{v} = \sum(\bar{x} - \bar{R}_i)\bar{q}_i/(\|\bar{x} - \bar{R}_i\|^2)$. The dimensionless controller equations are solved using ACADO (*SI Appendix, SI Text, 1.3. Controller Implementation*).

**ACKNOWLEDGMENTS.** We thank Prof. Sascha Hilgenfeldt for insightful discussions. We thank Prof. Paul J. A. Kenis and his group for providing access to cleanroom facilities for microdevice fabrication. This work was supported by a FMC Educational Fund Fellowship (to A.S.), a Packard Fellowship from the David and Lucile Packard Foundation, and National Science Foundation (NSF) Faculty Early Career Development (CAREER) Award Chemical, Bioengineering, Environmental, and Transport Systems (CBET) 1254340 (to C.M.S.).

1. Ashkin A, Dziedzic JM, Bjorkholm JE, Chu S (1986) Observation of a single-beam gradient force optical trap for dielectric particles. *Opt Lett* 11(5):288.
2. Chiou PY, Ohta AT, Wu MC (2005) Massively parallel manipulation of single cells and microparticles using optical images. *Nature* 436(7049):370–372.
3. Neuman KC, Block SM (2004) Optical trapping. *Rev Sci Instrum* 75(9):2787–2809.
4. Gosse C, Croquette V (2002) Magnetic tweezers: Micromanipulation and force measurement at the molecular level. *Biophys J* 82(6):3314–3329.
5. Hertz HM (1995) Standing-wave acoustic trap for nonintrusive positioning of microparticles. *J Appl Phys* 78(8):4845–4849.
6. Ding X, et al. (2012) On-chip manipulation of single microparticles, cells, and organisms using surface acoustic waves. *Proc Natl Acad Sci USA* 109(28):11105–11109.
7. Cohen AE, Moerner WE (2008) Controlling Brownian motion of single protein molecules and single fluorophores in aqueous buffer. *Opt Express* 16(10):6941–6956.
8. Probst R, Cummins Z, Ropp C, Waks E, Shapiro B (2012) Flow control of small objects on chip: Manipulating live cells, quantum dots, and nanowires. *IEEE Control Syst* 32(2):26–53.
9. Tanyeri M, Johnson-Chavarria EM, Schroeder CM (2010) Hydrodynamic trap for single particles and cells. *Appl Phys Lett* 96(22):224101.
10. Tanyeri M, Ranka M, Sittipolkul N, Schroeder CM (2011) A microfluidic-based hydrodynamic trap: Design and implementation. *Lab Chip* 11(10):1786–1794.
11. Tanyeri M, Schroeder CM (2013) Manipulation and confinement of single particles using fluid flow. *Nano Lett* 13(6):2357–2364.
12. Chu S, Hollberg L, Bjorkholm JE, Cable A, Ashkin A (1985) Three-dimensional viscous confinement and cooling of atoms by resonance radiation pressure. *Phys Rev Lett* 55(1):48–51.
13. Selvin PR, Ha T, eds (2008) *Single-Molecule Techniques: A Laboratory Manual* (Cold Spring Harbor Laboratory Press, Cold Spring Harbor, NY).
14. Johnson-Chavarria EM, Agrawal U, Tanyeri M, Kuhlman TE, Schroeder CM (2014) Automated single cell microbioreactor for monitoring intracellular dynamics and cell growth in free solution. *Lab Chip* 14(15):2688–2697.
15. Taylor GI (1934) The formation of emulsions in definable fields of flow. *Proc R Soc Lond A Math Phys Sci* 146(858):501–523.
16. Bentley BJ, Leal LG (1986) A computer-controlled four-roll mill for investigations of particle and drop dynamics in two-dimensional linear shear flows. *J Fluid Mech* 167:219–240.
17. Schroeder CM, Babcock HP, Shaqfeh ESG, Chu S (2003) Observation of polymer conformation hysteresis in extensional flow. *Science* 301(5639):1515–1519.
18. Hudson SD, et al. (2004) Microfluidic analog of the four-roll mill. *Appl Phys Lett* 85(2):335–337.
19. Lee JS, Dylla-Spears R, Teclemariam NP, Muller SJ (2007) Microfluidic four-roll mill for all flow types. *Appl Phys Lett* 90(7):074103.
20. Shenoy A, Tanyeri M, Schroeder CM (2014) Characterizing the performance of the hydrodynamic trap using a control-based approach. *Microfluid Nanofluidics* 18(5-6):1055–1066.
21. Schneider TM, Mandre S, Brenner MP (2011) Algorithm for a microfluidic assembly line. *Phys Rev Lett* 106(9):094503.
22. Batchelor GK (2000) *An Introduction to Fluid Dynamics* (Cambridge Univ Press, Cambridge, UK).
23. Mayne DQ, Rawlings JB, Rao CV, Scokaert PO (2000) Constrained model predictive control: Stability and optimality. *Automatica* 36(6):789–814.
24. Houska B, Ferreau HJ, Diehl M (2011) ACADO toolkit—An open-source framework for automatic control and dynamic optimization. *Optim Control Appl Methods* 32(3):298–312.
25. Sbalzarini IF, Koumoutsakos P (2005) Feature point tracking and trajectory analysis for video imaging in cell biology. *J Struct Biol* 151(2):182–195.
26. Lansdorp BM, Saleh OA (2012) Power spectrum and Allan variance methods for calibrating single-molecule video-tracking instruments. *Rev Sci Instrum* 83(2):025115.
27. Yu Z, et al. (2014) A force calibration standard for magnetic tweezers. *Rev Sci Instrum* 85(12):123114.
28. Neuman KC, Nagy A (2008) Single-molecule force spectroscopy: Optical tweezers, magnetic tweezers and atomic force microscopy. *Nat Methods* 5(6):491–505.
29. Leal LG (2007) *Advanced Transport Phenomena: Fluid Mechanics and Convective Transport Processes* (Cambridge University Press, Cambridge).
30. Peterman EJG, Gittes F, Schmidt CF (2003) Laser-induced heating in optical traps. *Biophys J* 84(2 Pt 1):1308–1316.
31. Hecht S (2005) Construction with macromolecules. *Mater Today* 8(3):48–55.
32. Whitesides GM, Boncheva M (2002) Beyond molecules: Self-assembly of mesoscopic and macroscopic components. *Proc Natl Acad Sci USA* 99(8):4769–4774.
33. Vijayaraghavan A, et al. (2007) Ultra-large-scale directed assembly of single-walled carbon nanotube devices. *Nano Lett* 7(6):1556–1560.
34. Bevan MA, et al. (2015) Controlling assembly of colloidal particles into structured objects: Basic strategy and a case study. *J Process Contr* 27:64–75.
35. Xu F, et al. (2011) The assembly of cell-encapsulating microscale hydrogels using acoustic waves. *Biomaterials* 32(31):7847–7855.
36. Pantina JP, Furst EM (2004) Directed assembly and rupture mechanics of colloidal aggregates. *Langmuir* 20(10):3940–3946.